HHS Public Access

Author manuscript

J Med Chem. Author manuscript; available in PMC 2020 November 14.

Published in final edited form as:

J Med Chem. 2019 November 14; 62(21): 9743–9752. doi:10.1021/acs.jmedchem.9b01186.

Novel Matrix Metalloproteinase 12 selective radiotracers for vascular molecular imaging

Jakub Toczek[#,//], **Thomas Bordenave**[‡], **Kiran Gona**[#,//], **Hye-Yeong Kim**[#,//], **Fabrice Beau**[‡], **Dimitris Georgiadis**[§], **Isabelle Correia**[°], **Yunpeng Ye**[#,//], **Mahmoud Razavian**[#,//], **Jae-Joon Jung**[#,//], **Olivier Lequin**[°], **Vincent Dive**[‡], **Mehran M. Sadeghi**[#,//,*], **Laurent Devel**[‡,*]

[#] Cardiovascular Molecular Imaging Laboratory, Section of Cardiovascular Medicine and Yale Cardiovascular Research Center, Yale University School of Medicine, New Haven, CT-06511 (USA)

[//] Veterans Affairs Connecticut Healthcare System, West Haven, CT-06516 (USA)

[‡] CEA, Institut des Sciences du Vivant Frédéric Joliot, Service d'Ingénierie Moléculaire des Protéines (SIMOPRO), Université Paris-Saclay, Gif-sur-Yvette 91190, France.

[§] Department of Chemistry, Laboratory of Organic Chemistry, University of Athens, Panepistimiopolis Zografou, 15771, Athens, Greece.

[°] Sorbonne Université, Ecole Normale Supérieure, PSL University, CNRS, Laboratoire des Biomolécules, LBM, 75005 Paris, France

Abstract

Matrix metalloproteinase-12 (MMP-12) is highly upregulated in several inflammatory diseases, including abdominal aortic aneurysm (AAA). Here we report four novel ^{99m}Tc-labeled radiotracers derived from a highly selective competitive MMP-12 inhibitor. These tracers in their ^{99g}Tc version were assessed *in vitro* on a set of human metalloproteases and displayed high affinity and selectivity toward MMP-12. Their radiolabeling with ^{99m}Tc was shown to be efficient and stable in both buffer and mouse blood. The tracers showed major differences in their biodistribution and blood clearance. Based on its *in vivo* performance, [^{99m}Tc]-**1** was selected for

[*]Corresponding authors: Laurent Devel. Phone: +33 169089565; Fax: +33169089071; laurent.devel@cea.fr., Mehran M. Sadeghi. Phone: 203 737 6954; Fax: 203 937 3884; mehran.sadeghi@yale.edu.

Author Contributions

The manuscript was written through contributions of all authors.

Notes

All authors have given approval to the final version of the manuscript. The authors declare no competing financial interest.

ASSOCIATED CONTENT

Supporting information

Inhibitory Constant (Ki) of [^{99g}Tc]-**1**, [^{99g}Tc]-**2**, [^{99g}Tc]-**3** and [^{99g}Tc]-**4** towards a set of metzincins

IC_{50} of RXP470.1 and RXP470.1-derived compounds [^{99m}Tc] **1-4** towards hMMP12 in presence of human Serum Albumin (hSA), mouse (mSA) or mouse plasma. Log P of compounds [^{99m}Tc] **1-4** determined in Octanol/PBS (1/1)

Statistical analysis of the tracers' blood kinetics and biodistribution

^{1}H and ^{13}C NMR assignments of compounds **5**, **6**, **7** and **8**

Tracer biodistribution and clearance of [^{99m}Tc]-**1**

Representative ^{1}H, 2D HSQC ^{13}C-^{1}H and 2D HMBC ^{13}C-^{1}H NMR spectra for compounds compounds **5**, **6**, **7** and **8**

Representative ^{1}H NMR spectra for compounds compounds [^{99g}Tc] **1-4**

RP-HPLC profiles and MS spectra of compounds **5**, **6**, **7**, **8** as well as [^{99g}Tc] **1-4** derivatives

Molecular formula strings (CSV).

evaluation in murine AAA, where MMP-12 gene expression is upregulated. Autoradiography of aortae at two hours post-injection revealed high uptake of [^{99m}Tc]-**1** in AAA relative to adjacent aorta. Tracer uptake specificity was demonstrated through *in vivo* competition. This study paves the way for further evaluation of [^{99m}Tc]-**1** for imaging AAA and other MMP-12-associated diseases.

Graphical Abstract

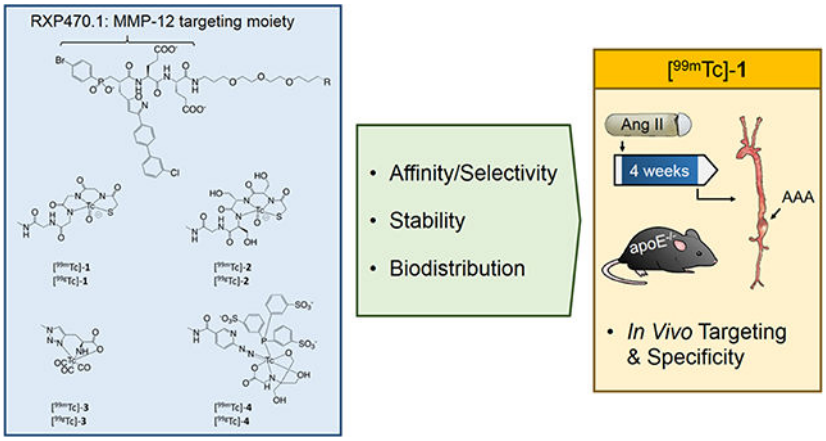

INTRODUCTION

Matrix metalloproteinases (MMPs) are a family of calcium-dependent zinc-containing endopeptidases that belongs to the metzincin superfamily. MMPs are secreted as inactive zymogens that require proteolytic activation and their activity is regulated by the presence of tissue inhibitors.[1] Members of the MMPs family have a broad range of substrates with variable specificity.[2] MMPs have been implicated in numerous physiological and pathological processes, and play complex roles in tissue inflammation and inflammation resolution.[3, 4]

MMP-12, also named macrophage elastase, is best known for its ability to cleave elastin,[5, 6] a major component of elastic laminae in the media of arteries. Macrophages are major sources of MMP-12.[7] As such, MMP-12 is upregulated in several inflammatory diseases, including abdominal aortic aneurysm (AAA), atherosclerosis, and chronic obstructive pulmonary disease (COPD). While normal arteries express low levels of MMP-12, MMP-12 is highly expressed in human AAA, where it can be detected in association with residual medial elastic fibers.[8] This observation is replicated in the mouse, where aneurysm induction leads to significant MMP-12 expression in the arterial wall.[9, 10] Importantly, several preclinical studies have indicated that MMP-12 plays a major role in AAA development and potentially rupture.[10–13] MMP-12 is also expressed in atherosclerosis, and based on its association with adverse cardiovascular events, has been proposed as a biomarker for atherosclerotic plaque vulnerability.[8, 14] Similarly, MMP12 is upregulated and may play a role in inflammatory lung diseases such as COPD[15, 16] and asthma.[17] Taken together, these findings suggest that the presence of active MMP-12 may constitute a biomarker in various inflammatory diseases. Particularly, probing the *in vivo* activation of this enzyme may allow

to grade the pathological state and define the temporal window during which MMP-12 could be considered as a potential therapeutic target.

Given the role of MMP activation in the pathogenesis of several inflammatory diseases, MMP activity may represent a promising therapeutic target. However, in part due to the complexity of the actions of the different MMPs, several broad spectrum MMP inhibitors have failed in clinical trials.[18] This led to the development of highly selective MMP inhibitors.[19–24] Among them, the phosphinic pseudo peptide RXP470.1 (Figure 1) was identified as a highly potent competitive inhibitor able to selectively target MMP-12.[25] MMP-12 specific inhibition with RXP470.1 has been validated in six different preclinical models,[26–31] suggesting that this inhibitor may be considered as a relevant starting point for the development of MMP-12-selective imaging agents.

Based on the structure of RXP470.1, MMP-12-specific optical probes were recently developed[9, 10] and their *in vivo* performances evaluated in a model of aneurysmal arterial remodeling.[10] In this series of compounds, it was demonstrated that fluorescent reporters impacted probe pharmacokinetics and biodistribution. Particularly, the probes' non-specific binding to serum albumin could be subtly tuned by the chemical nature of the fluorophore with non-negligible impact on probe accumulation within the tissue of interest. While of great value for basic research and potentially certain preclinical studies, the inherent limitations of optical imaging preclude the application of fluorescent probes for non-invasive imaging in humans. Unlike optical imaging, nuclear imaging is routinely used in the clinic. In this respect, very recent studies have led to the development of MMP-12 radiotracers incorporating in their structure a fluorine 18 radioisotope for positron emission tomography[32, 33] and radioiodinated MMP-12 probes.[34] Here, we describe the development and evaluation of RXP470.1-derived tracers labeled with ^{99m}Tc for nuclear imaging. These novel tracers share a common MMP-12-targeting moiety conjugated to a short PEG spacer to prevent eventual steric clashes during binding to the target and differ in their Tc chelating groups (Figure 1). After synthesis and radiolabeling, the binding properties of ^{99g}Tc labeled tracers were assessed towards a set of twelve human metalloproteases as well as murine MMP12. The radiochemical stability of ^{99m}Tc-labeled tracers was then evaluated, and the tracers' pharmacokinetics and biodistribution were compared. The tracer displaying the best performance was tested in a mouse model of AAA in which MMP-12 is upregulated.[35] Finally, the specificity of the tracer uptake was confirmed through competition experiments in the presence of a broad-spectrum MMP inhibitor.

RESULTS

Synthesis of precursors 5, 6, 7 and 8

Radiotracers **1**, **2**, **3** and **4** were obtained from precursors **5**, **6**, **7**, and **8** respectively (Scheme 1). Briefly, pseudo peptide scaffold **I** was generated on resin from a phosphinic building block using standard Fmoc strategy as previously described.[9] After a selective removal of Monomethoxy trityl (Mmt) protecting group, a *C*-terminal extension on the resulting free amino function was performed by incorporating either two Fmoc-Gly-OH or two Fmoc-Ser(OtBu)-OH units successively. These steps were followed by a conjugation step with *N*-hydroxysuccinimide activated S-Acetylthioglycolic acid yielding, after cleavage from the

support and RP-HPLC purification, precursor **5** (20%) and **6** (10%). Derivative **II** was obtained after cleavage and RP-HPLC purification as described.[9] The free amino function of **II** was first transformed into azido function in presence of imidazole sulfonyl azide trifluoroborate salt and copper sulfate. After 24h, the reaction completion was confirmed by LC/MS and the resulting azido derivative was directly engaged in a Cu-catalyzed 1,3-dipolar cycloaddition with propargyl glycine. After 30 min under microwave irradiation (60 °C, 25 W), the crude mixture was purified by RP-HPLC to afford **7** (60%). From the same intermediate **II**, precursor **8** (47%) was obtained after a coupling step with Succinimidyl 6-(BOC-hydrazine)-nicotinate[36] followed by a RP-HPLC purification.

Reagents and conditions: (a) Fmoc-Glu(OtBu)-OH (10 equiv), ClHOBt/DIC (10 equiv), DMF, 60°C, microwave irradiation at 45W, 10 min, (b) Phosphinic building block **A** (1.2 equiv), ClHOBt/DIC (3 equiv), DMF, 60°C, microwave irradiation at 45W, 60 min, (c) 0.6 M HOBt (TFE/DCM: 1/1), RT, 30 min, (d) Fmoc-X-OH X= Gly (5equiv) or Ser(OtBu), HCTU (5equiv), NMM (5equiv), NMP ([C]=0.02M), 60°C, microwave irradiations at 45W, 10 min, followed by addition of S-Acetylthioglycolic acid N-hydroxysuccinimide ester (3equiv), DIEA (5equiv), in DMF ([C]=0.05M). RT, 12h, (e) TFA/TIS/H_2O: 95/2.5/2.5, RT, 3×45 min, (f) RP-HPLC purification affording **5** and **6** with 20% and 10% yield respectively, (g) TFA/TIS/H_2O: 95/2.5/2.5, RT, 3×45 min followed by RP-HPLC purification, (h) Compound **II** (1 equiv), $CuSO_4$ (2.8 equiv), Imidazole-1-sulfonyl azide tetrafluoroborate (20 equiv), carbonate buffer 50 mM/Methanol (3:1), pH = 8.5, RT, 24h, followed by addition of L-propargyl glycine (50 equiv), sodium ascorbate (35 equiv), $CuSO_4$ (2.8 equiv), 60°C, microwave irradiation at 45W, 30 min, (i) RP-HPLC purification affording **7** with 60% yield, (j) Compound **II** (1 equiv), succinimidyl 6-(boc-hydrazine)nicotinate (2 equiv), dry DMF, RT, 16h, followed by DMF removal under reduced pressure and dilution in HCl_{aq} (5M), RT, 24h, (k) RP-HPLC separation affording **8** with 47% yield.

Radiosynthesis of [^{99m}Tc] and [^{99g}Tc] derivatives

Precursors **5**, **6**, **7** and **8** were labeled with ammonium pertechnetate $^{99g}[TcO_4^-NH_4^+]$ according to procedures described in experimental section. [^{99g}Tc]-**1** to **4** were isolated with >95% purity after RP-HPLC (see SI for details). Radiolabeling with ^{99m}Tc was performed following procedures similar to previously described methods for MAG, MAS, Triazole and HYNIC conjugated compounds[37–39] with empirical adjustments for the different compounds and methods. Without any post-labeling chromatographic purification, the radiochemical purity of the resulting ^{99m}Tc-labeled compounds was >95%. The specific activities of [^{99m}Tc]-**1**, **2**, **3** and **4** were 21–126 GBq/μmol, 14–94 GBq/μmol, 17–74 GBq/μmol and 26–41GBq/μmol, respectively.

Ki determination of [^{99g}Tc]-1 to 4 derivatives towards a set of metalloproteases

For each derivative, the inhibition constant was *in vitro* evaluated through an inhibition assay in presence of a fluorogenic substrates.[9] As shown in figure 2, compounds [^{99g}Tc]-**1** to **4** displayed Ki values towards hMMP12 comparable to that of parent RXP470.1, ranging from 0.2 nM for the HYNIC derivative **4** to 1.9 nM in the case of MAS compound **1**. The binding capacity of these compounds towards murine MMP-12 was maintained by comparison to parent molecule, with inhibition constant ranging 0.4 to 20 nM (Figure 2 and Table S1).

More importantly, the joint presence of PEG spacer and Tc chelating moiety impacted the selectivity profile of RXP470.1-derived probes only moderately, which remained favorable for hMMP12.

In addition, inhibition constants of [^{99g}Tc]-**1** to **4** towards hMMP-12 were reduced in the presence of human or mouse serum albumin, and further decreases were observed while incubated in different dilutions of mouse plasma (Table S2). In mouse plasma, this drop in affinity ranged from three (factor 600 for [^{99g}Tc]-**3**) to four orders of magnitude (factor 3500 for [^{99g}Tc]-**4**). This shift in potency was also observed for parent RXP470.1 (factor 470 in mouse plasma). The propensity to bind human and mouse serum albumin was comparable for the four derivatives. All ^{99g}Tc radiolabeled compounds were hydrophilic with octanol/PBS partition coefficient ranging from −1.1 to −2.3 (Table S2).

Radiolabeling stability

We then investigated the radiochemical stability of [^{99m}Tc]-**1** to **4** compounds in PBS. As shown in Figure 3, after 6 hours of incubation at room temperature, no significant evolution of the radio-HPLC profile of tracers [^{99m}Tc]-**1**, [^{99m}Tc]-**2** and [^{99m}Tc]-**3** was observed, demonstrating an excellent radiochemical stability in these conditions. The analysis of [^{99m}Tc]-**4** by radio-HPLC was unsuccessful due to high retention within the fluidic component of the system with a wide range of testing conditions.

Similar experiments were performed in mouse blood for up to 3 h of incubation at 37°C. Samples were collected at three different time points (0.5 h, 2 h and 3 h) and analyzed by radio-HPLC (Figure 4). The three tracers appeared fully stable in these conditions with no detectable degradation compounds generated within the three hours of incubation.

Biodistribution studies

The pharmacokinetics and biodistributions of the four ^{99m}Tc-labeled compounds were then evaluated in C57BL/6J-albino mice. As illustrated by Figure 5, tracers [^{99m}Tc]-**1** and [^{99m}Tc]-**3** showed fast blood clearance with blood levels at 2 h post-injection (p.i.) 1.9 ± 0.8 and 2.1 ± 0.4 %injected dose (ID)/mL, respectively, while with 12.3 ± 1.5%ID/mL, [^{99m}Tc]-**4** had the highest residual blood activity at 2 h p.i. (Figure 5A). Compounds [^{99m}Tc]-**1**, [^{99m}Tc]-**2** and [^{99m}Tc]-**3** showed mix hepato-biliary and renal clearance, with high activity in both bile and urine, while [^{99m}Tc]-**4** showed a preferential urinary excretion, with only modest bile activity. Uptake of [^{99m}Tc]-**4** was elevated in lungs, liver, spleen [19–23 %ID)/g] and kidneys (33 %ID/g). Uptake of [^{99m}Tc]-**1** and [^{99m}Tc]-**3** was low in non-diseased aorta (1.7 ± 0.4 and 2.0 ± 0.6 %ID/g, respectively) and perivascular adipose tissue (1.1 ± 0.2 and 1.4 ± 1.0 %ID/g, respectively).

Uptake in those tissues was higher with the two other tracers [^{99m}Tc]-**2** and [^{99m}Tc]-**4** (Figure 5B, and Table S3). These data highlighted the influence of Tc chelating moiety on pharmacokinetics of the tracers with the MAG derivative [^{99m}Tc]-**1** offering the most favorable properties both in terms of blood clearance and uptake in normal aorta.

Evaluation of [^{99m}Tc]-1 in AAA and specificity

Based on its *in vivo* performance, [^{99m}Tc]-**1** was selected for testing in a murine model of angiotensin (Ang) II-induced AAA. We have previously shown that Ang II infusion in apolipoprotein (Apo)E$^{-/-}$ mice leads to the development of AAA in a subset of animals, and MMP-12 expression is significantly upregulated in AAA in this model.[35] As expected, Ang II infusion in male ApoE$^{-/-}$ mice (n=23) led to death from aneurysm rupture in eight (35%) of the animals before the 4-week time point used for imaging. In the surviving animals, the incidence of AAA was 47% (7/15). [^{99m}Tc]-**1** (20.6 ± 5.6 MBq) was injected intravenously to the surviving mice and the animals were subsequently sacrificed at 2 h p.i. for autoradiography. Quantitative analysis of the images showed that [^{99m}Tc]-**1** uptake in AAA was 1.7-fold higher compared to adjacent infra-renal aorta ($P < 0.05$). Pre-injection of a 1000-fold excess of RYM, a broad-spectrum MMP inhibitor[40] resulted in a 3.6-fold decrease in [^{99m}Tc]-**1** uptake in aneurysm, demonstrating uptake specificity. Of note, the [^{99m}Tc]-**1** signal was decreased 3.0-fold in the normal-appearing aorta in blocking experiments, reflecting diffuse aortic activation of MMP-12 in this model (Figure 6). Notably, unlike tracer uptake in AAA, only minor differences existed in [^{99m}Tc]-**1** blood kinetics and tissue biodistribution between non-blocking and blocking conditions (Figure S1).

DISCUSSIONS AND CONCLUSIONS

We report the design and development of a new family of ^{99m}Tc-labeled MMP-12 tracers structured based on the selective MMP-12 inhibitor, RXP470.1. The tracers were shown to retain high affinity and selectivity for MMP-12. Combining blood clearance, biodistribution and affinity/selectivity profiles, [^{99m}Tc]-**1** was selected as the leading compound for *in vivo* evaluation in a murine model of AAA with MMP-12 upregulation.[13, 35] In this model, there was higher uptake of [^{99m}Tc]-**1** in AAA compared to non-aneurysmal aorta, and blocking experiments established MMP-specificity of this higher uptake in AAA *in vivo*.

The design of MMP-12-specific radiotracers were in part based on the information gained from the recently-described MMP-12 optical probes.[9, 10] In this case, we have demonstrated that it was possible to conjugate various fluorescent moieties at the C-terminal end of RXP470.1 pseudo peptide with only minimal impact on affinity and selectivity towards MMP-12 for the resulting constructs.[9] Further, we have clearly showed that the chemical nature of fluorophores, specifically their global charge, significantly affected the RXP470.1-derived probes' binding to serum albumin with consequences on probes' pharmacokinetics and biodistribution. By relying on these observations, we inserted four ^{99m}Tc chelating groups of different core structures at the C-terminal end of RXP470.1. Indeed, it was recently demonstrated that in the case of radiopharmaceuticals targeting Prostate-Specific Membrane Antigen (PSMA), the choice of the Tc-chelating cage is critical for achieving optimized *in vivo* performance of imaging agents.[41] In the RXP470.1 series, we thus explored the traditional ^{99m}Tc-oxo core with a tetradentate N_3S-based chelator (MAG ^{99m}Tc-**1** and MAS ^{99m}Tc-**2** tracers), the ^{99m}Tc-tricarbonyl core (^{99m}T-**3**) and the ^{99m}Tc-hynic core (^{99m}Tc-**4**). These different Tc-chelating moieties led to radiotracers with different overall charge, lipophilic character and stability with potential consequences on their binding properties, pharmacokinetics and MMP-12-targeting capacities.

The shift in tracers' affinity to MMP-12 in mouse plasma dilutions reflected the propensity of RXP470.1-derived compounds to interact with other proteins than the targeted MMP-12. Further, the observations made in the presence of serum albumin suggested that this protein was the main binder for the tracers, which was consistent with the results obtained with optical probe series. Of note, this phenomenon occurred in a similar extent for the parent RXP470.1 and its derived tracers, as evidenced by their comparable shift of IC_{50} (Table S2). This observation needs to be considered for both imaging and enzymatic inhibition purposes. Indeed, the apparent decrease in tracers' affinity in the plasma may adversely affect the quality of *in vivo* images. This issue will be the subject of future studies.

The selection of [^{99m}Tc]-**1** as the lead compound was based on its favorable pharmacokinetics profile, showing a combination of low blood activity at 2 h p.i. and less uptake in tissues surrounding the aorta. Furthermore, although these differences were not significant, [^{99m}Tc]-**1** showed a 2.7-fold higher affinity for murine MMP-12 compared to [^{99m}Tc]-**3**, while the affinity for human MMP-12 was comparable, which favored its use in the mouse model. Tracer clearance kinetics are especially important for vascular imaging, where the proximity of the vessel wall and blood mandates the use of tracers with rapid blood pool clearance to yield sufficient contrast between the blood and the arterial wall. Tracers **1**, **2**, and −**3** were radiochemically stable *in vitro* for up to 3 h in mouse blood. Blocking experiments suggest that [^{99m}Tc]-**1** should be stable, at least at the tissue level, *in vivo*. However, in the absence of empiric data, the *in vivo* radiochemical stability of different tracers cannot be ascertained. The 2 h time-point selected to assess tissue biodistribution, represents a practical compromise for imaging in humans, and is consistent with previous studies with MMP tracers. Future in vivo imaging studies should provide more detailed analysis of tracer biokinetics.

We have previously shown that MMP-12 gene expression is significantly upregulated in Ang II-induced AAA compared to normal aorta[35] or aortae from Ang II-infused animals with only modest remodeling.[13] In the current study, we observed 1.7-fold higher [^{99m}Tc]-**1** uptake in AAA compared to non-aneurysmal aorta from same animal. Of note, analysis of tracer uptake by digital autoradiography does not permit the preservation of the tissue for subsequent tissue analysis. Therefore, we could not assess MMP-12 gene or protein expression or MMP-12 activity to correlate with tracer uptake in AAA. However, the MMP-specificity of [99mTc]-**1** uptake was demonstrated by blocking of the signal in the presence of an excess of the inhibitor. Although a direct comparison of two different imaging modalities may be questionable, the range of tracer uptake in aneurysm in relation to control tissue was somewhat lower compared to the uptake ratio obtained with fluorescent probes using the same targeting moiety in a model of carotid aneurysm.[10] There are key differences in the animals models which may explain this difference; the location (carotid vs aorta) and trigger (calcium chloride vs Ang II) of aneurysm, as well as the reference artery which in the case of carotid aneurysm is the saline-treated contralateral carotid artery, but in the case of Ang II-induced AAA is the adjacent aorta with low remodeling (which is not necessarily normal). In addition, we cannot rule out that despite similar in vitro performance of the tracers, the physicochemical properties and interactions in the biological milieu may have affected the signal.

This study reports the generation and evaluation of the first ^{99m}Tc-labeled radiotracers that selectively target MMP-12. The lead compound displayed specific *in vivo* uptake in a preclinical model of AAA. With the wide range of pathologies associated with MMP-12 upregulation and the advantages of nuclear imaging modalities, this tracer could be a valuable tool for pathophysiological research and clinical translation.

EXPERIMENTAL SECTION

1. Synthetic Chemistry

1.1. Chemical Reagents and procedures—Commercially available reagents and solvents were used as received without further purification. Diisopropylcarbodiimide (DIC), 1-Hydroxybenzotriazole hydrate (HOBt), Trifluoroacetic acid (TFA), *O*-(6-Chlorobenzotriazol-1-yl)-*N*,*N*,*N*′,*N*′-tetramethyluronium hexafluorophosphate (HCTU), *N*-methylmorpholine (NMM), *N*-methyl pyrrolidone (NMP), N,N-diisopropylethylamine (DIEA), S-Acetylthioglycolic acid N-hydroxysuccinimide ester, Triisopropylsilane (TIS), Trifluoroethanol (TFE), imidazole sulfonyl azide trifluoroborate salt, and 3,3′,3″-Phosphanetriyltris(benzenesulfonic acid) trisodium salt were purchased from Sigma-Aldrich (USA). The Universal PEG NovaTag™ resin (100–200 Mesh, 0,9 mmol/g) and Fmoc-AA-OH were purchased from Merck (Germany). 6-Chloro-1-Hydroxybenzotriazole (ClHOBt) was purchased from Molekula (United Kingdom). Succinimidyl 6-(boc-hydrazine)nicotinate was synthesized from 6-chloronicotinic acid (Aldrich) according to a procedure previously reported.[36] The pseudo peptide syntheses were performed manually using a polypropylene syringe (Supelco) equipped with a polyethylene frit and a stopper. The microwave experiments were performed with a Discover apparatus (CEM μWave, Matthews, NC, USA) using the open vessel mode with a SPS kit. Ammonium per technetate $^{99g}[TcO_4^-NH_4^+]$ was purchased from the National Oak Ridge laboratory (USA). DO measurements were performed on a Shimadzu UV spectrophotometer (UV-1800). The analytical RP-HPLC separations were performed in i) Condition A: 0–10 min: 0–100%B, with H_2O/0.1%TFA (v/v) as solvent A and acetonitrile/0.09%TFA (v/v) as solvent B, Supelco Ascentis express C_{18} column (2.7μ 150 × 4.6 mm, 1,2 mL.min^{-1}), UV detection at 230–280 nm, ii) Condition B: 0–10 min: 0–100%B, with H_2O/0.1%TFA (v/v) as solvent A and acetonitrile/0.09%TFA (v/v) as solvent B, Grace HT C_{18} HL column (5μ 150 × 4.6 mm, 1,2 mL.min^{-1}), UV detection at 230–280 nm, iii) Condition C: 0–20 min: 0–100%B with H_2O/0.1%TFA (v/v) as solvent A and acetonitrile/0.09%TFA (v/v) as solvent B, Grace HT C_{18} HL column (5μ 150 × 4.6 mm, 1 mL.min^{-1}), UV detection at 230–280 nm, iv) Condition D: 0–20 min: 0–100%B with 25 mM ammonium formate-H_2O as solvent A and ACN-10% 25 mM ammonium formate as solvent B, Grace HT C_{18} HL column (5μ 150 × 4.6 mm, 1,2 mL.min^{-1}), UV detection at 230–280 nm, or v) Condition E: 0–20 min: 0–100%B with 25 mM ammonium formate-H_2O as solvent A and ACN-10% 25 mM ammonium formate as solvent B, Grace HT C_{18} HL column (5μ 150 × 4.6 mm, 0,6 mL.min^{-1}), UV detection at 230–280 nm. The semi-preparative RP-HPLC purifications were performed in condition 1: 0–30 min: 0–100%B, with H_2O/0.1%TFA (v/v) as solvent A and acetonitrile/0.09%TFA (v/v) as solvent B, Supelco Ascentis® C18 column (10 × 250 mm, 10 μm, 3 mL.min^{-1}), UV detection at 230–280 nm. The retention times (Rt) were reported in minutes (min). The NMR experiments were acquired on a Bruker Avance III 500 MHz spectrometer equipped

with a TCI $^{1}H/^{13}C/^{15}N$ cryoprobe. The spectra of precursors **5** to **8** were recorded in DMSO-d_6 at 298 K using 200 μL samples in 3 mm NMR tubes (**5** and **7**) or 250 μL samples in 5 mm Shigemi NMR tubes (**6** and **8**). Complete ^{1}H, ^{13}C assignments were obtained from the analysis of 1D ^{1}H, 1D ^{13}C DEPTQ, 2D ^{1}H-^{1}H TOCSY, 2D ^{1}H-^{1}H ROESY, 2D ^{1}H-^{13}C HSQC and 2D ^{1}H-^{13}C HMBC experiments. The 1D ^{1}H spectra were recorded on compounds [^{99g}Tc]-**1** to **4** in D_2O using 5 mm Shigemi tubes. The mass spectrometry data were registered using a 4800 MALDI-TOF mass spectrometer (Applied Biosystems, Foster City, CA, USA) or an ion trap Esquire HCT spectrometer (Bruker Daltonics, Billerica, MA, USA). The amino acid compositions were performed on an aminoTac JLC-500/V amino acids analyser (JEOL, Tokyo, Japan). The identity and purity of each newly synthesized compound were assessed by analytical RP-HPLC (two different conditions, see supplemental information for representative chromatograms), NMR (^{1}H and ^{13}C for compounds **5**, **6**, **7** and **8** and ^{1}H for compounds [^{99g}Tc]-**1** to **4**, see supplemental information for representative NMR spectra) and mass spectrometry. Each target compound displayed a purity >95%.

1. 2. Compound Synthesis and characterization

1. 2. 1. Synthesis of ^{99g}[TcO4^{-}NH4^{+}]: Ammonium per technetate ^{99g}[TcO4^{-}NH4^{+}] was re-oxidized as described.[42] The concentration of aqueous solution was determined by UV considering an extinction coefficient of $\varepsilon_{244\ nm} = 5690\ cm^{-1}M^{-1}$.

1. 2. 2. Procedure to access [^{99g}Tc]-1 and 2: A solution of **5** or **6** (50 nmol) in ammonium acetate buffer (0.4 M, pH= 8, 125 μL) was mixed with a freshly prepared $SnCl_2$ solution in sodium ascorbate buffer (4 mg/mL, pH= 8.5, 20 μL). A solution of ^{99g}Tc-pertechnetate (1 μL of 33mM solution, 33 nmol, 0.7 equiv) was added and the reaction mixture was heated at 100 °C for 20 min. The crude compounds were purified by RP-HPLC in condition A affording pure [^{99g}Tc]-**1** (24 nmol, 48%) and [^{99g}Tc]-**2** (28 nmol, 56%) as white powders after freeze-drying.

Compound [^{99g}Tc]-1: $\varepsilon_{272\ nm}$(MeOH) = 41 606 $cm^{-1}M^{-1}$. Rt = 6.43 min in condition A. LC/MS Analysis (condition C), Rt = 15.33 min. The ^{1}H NMR spectrum of the compound [^{99g}Tc]-**1** was registered in D_2O with pre-saturation of the solvent (Figure S14) with no assignment in this case. MS (ESI) m/z for $[C_{55}H_{68}BrClN_9O_{19}PSTc]^{+}$, calcd: 1436.5; found: 1436.2

Compound [^{99g}Tc]-2: $\varepsilon_{272\ nm}$(MeOH) = 42 755 $cm^{-1}M^{-1}$. Rt = 6.21 min in condition A. LC/MS Analysis (Condition C): Rt = 15.06 min. The ^{1}H NMR spectrum of the compound [^{99g}Tc]-**2** was registered in D_2O with pre-saturation of the solvent (Figure S15) with no assignment in this case. MS (ESI) m/z for $[C_{58}H_{74}BrClN_9O_{22}PSTc]^{+}$, calcd: 1526.6; found: 1526.3.

1. 2. 3. Procedure to access [^{99g}Tc]-3: In a sealed tube, sodium boronocarbonate (0.45 mg, 4.6 μmol), a water solution of borax (29 mg/mL, 10μL), a water solution of sodium tartrate (85 mg/mL, 10μL), a water solution of calcium carbonate (8mg/mL, 10μL) and a solution of ^{99g}Tc-pertechnetate (50 nmol, 33 mM, 1.5 μL, 5 equiv) were successively added.

The reaction mixture was heated at 100°C for 10 min. After cooling down to room temperature, the pH was adjusted to ~ 8–8.5 with a solution of HCl (330 mM, 20 μL) and a water solution of **7** was added (10 nmol, 1M, 10μL). The reaction was carried out at 100°C for 20 min. The crude reaction mixture was then purified by RP-HPLC in condition A affording a pure [^{99g}Tc]-**3** (4.3 nmol, 43%) as a white powder after freeze-drying.

Compound [^{99g}Tc]-3: $\varepsilon_{272\ nm}$(MeOH) = 39 735 $cm^{-1}M^{-1}$. Rt = 7.02 min in condition A. LC/MS Analysis (Condition C): Rt = 19.44 min. The ^{1}H NMR spectrum of the compound [^{99g}Tc]-**3** was registered in D_2O with pre-saturation of the solvent (Figure S16) with no assignment in this case. MS (ESI) m/z for $[C_{53}H_{60}BrClN_8O_{18}PTc]^+$, calcd: 1342.3; found: 1343.3

1. 2. 4. Procedure to access [^{99g}Tc]-4: A solution of **8** (70 μg, 30 nmol) in sodium carbonate buffer (500 mM, pH= 7.8, 75 μL) was combined to a water solution of tricine (3.9 μmol, 56 mM, 70 μL, 130 equiv). To this solution a DMSO solution of 3,3′,3″-Phosphanetriyltris(benzenesulfonic acid) trisodium salt (3.4 μmol, 500 mM, 7 μL, 114 equiv) and a solution of ^{99g}Tc-pertechnetate (33 nmol, 33 mM, 1 μL, 1.1 equiv) were successively added. The reaction mixture was heated at 100 °C for 10 min under microwave irradiations (25W). The crude reaction mixture was purified by RP-HPLC in condition D to afford a pure [^{99g}Tc]-**4** (14 nmol, 47%) as a white powder after freeze drying.

Compound [^{99g}Tc]-4: $\varepsilon_{272\ nm}$(MeOH) = 58 670 $cm^{-1}M^{-1}$. Rt = 8.66 min in condition D. LC/MS Analysis (Condition E): Rt = 8.65 min. The ^{1}H NMR spectrum of the compound [^{99g}Tc]-**4** was registered in D_2O with presaturation of the solvent (Figure S17) with no assignment in this case. MS (ESI) m/z for $[C_{75}H_{85}BrClN_9O_{28}P_2S_3Tc]^+$, calcd: 1932.9; found: 1932.3

1. 2. 5. Solid phase synthesis of precursors 5 and 6: A standard Fmoc methodology was used to build amino acid sequence on Universal PEG NovaTagTM resin (300 mg, 0.074 mmol). Fmoc-Glu(OtBu)-OH (0.315 g, 0.74 mmol, 10 equiv) and the phosphinic building block A (0.062 g, 0.089 mmol, 1.2 equiv) were incorporated on solid support following a standard protocol in the presence of DIC and ClHOBt in DMF, as previously described.[9] To achieve the synthesis of compounds **5** and **6**, an additional elongation step on the amino function at the C-terminal position was implemented. The compound **I**[9] conjugated to the resin (57 mg, 11.5 μmol) was treated with a solution of 0.6 M HOBt in TFE/DCM: 1/1 at room temperature for 30 min. After washing steps with DMF (2 × 5 min) and DCM (2 × 5 min), an elongation of the free amino function was performed with either Fmoc-Gly-OH (5 equiv) or Fmoc-Ser(OtBu)-OH (5 equiv) pre-activated in presence of HCTU (5 equiv) and NMM (5 equiv) in NMP ([C]=0.02M). The coupling reaction was carried out under microwave irradiations (45W) at 60°C for 10 min. After the washing steps and Fmoc removal, S-Acetylthioglycolic acid N-hydroxysuccinimide ester (3 equiv) in DMF ([C]=0.05M) was coupled to the free amino function in the presence of DIEA (5equiv). The coupling reaction was conducted overnight at room temperature. The compounds **5** or **6** were then cleaved from the support with a TFA/TIS/H_2O: 95/2.5/2.5 cocktail (5 mL, 3 × 45

min). The crude pseudo peptides as a diastereomer mixture were purified by RP-HPLC in condition 1.

Compound 5 was obtained as white powder (3.1 mg, 20%) after freeze drying. $\varepsilon_{272\ nm}$(MeOH) = 34 820 $cm^{-1}M^{-1}$. Rt = 6.43 min in condition A, Rt = 7.32 min in condition B. The complete ^{1}H and ^{13}C NMR assignments are detailed in Table S4 (see also Figure S2, S3 and S4 for representative ^{1}H, 2D HSQC ^{13}C-^{1}H and 2D HMBC ^{13}C-^{1}H NMR spectra respectively). MS (MALDI-TOF) m/z for $[C_{57}H_{71}BrClN_9O_{19}PS]^-$, calcd: 1362.3202; found: 1362.4579.

Compound 6 was obtained as white powder (1.6 mg, 10%)) after freeze drying. $\varepsilon_{272\ nm}$(MeOH) = 34 360 $cm^{-1}M^{-1}$. Rt = 6.25 min in condition A, Rt = 7.28 min in condition B. Complete ^{1}H and ^{13}C NMR assignments are detailed in Table S5 (see also Figure S5, S6 and S7 for representative ^{1}H, 2D HSQC ^{13}C-^{1}H and 2D HMBC ^{13}C-^{1}H NMR spectra respectively). MS (MALDI-TOF) m/z for $[C_{60}H_{77}BrClN_9O_{22}PS$-], calcd: 1452.3519; found: 1452.5046.

1. 2. 6. Synthesis of precursor 7: To a solution of compound **II**[9] (1 mg, 1μmol) in carbonate buffer 50 mM/Methanol: 3/1 (1 mL, pH = 8.5) were added copper sulfate (0.7mg, 2.8 μmol, 2.8 equiv) and imidazole sulfonyl azide trifluoroborate salt (5.1 mg, 20 μmol, 20 equiv). The resulting blue solution was stirred at room temperature for 24h. The L-C-propargyl glycine (5.6 mg, 50 μmol, 50 equiv) and sodium ascorbate (6.9 mg, 35 μmol, 35 equiv) as well as a supplementary portion of copper sulfate (0.7mg, 2.8 μmol, 2.8 equiv) were then added. The reaction mixture was heated at 60°C for 30 minutes under microwave irradiations (25W). The crude pseudo peptide was purified by RP-HPLC in condition 1.

Compound 7 was obtained as white powder (0.76 mg, 60%) after freeze drying. $\varepsilon_{272\ nm}$(MeOH) = 33 023 $cm^{-1}M^{-1}$. Rt = 6.23 min in condition A, Rt = 7.38 min in condition B. The complete ^{1}H and ^{13}C NMR assignments are detailed in Table S6 (see also Figure S8, S9 and S10 for representative ^{1}H, 2D HSQC ^{13}C-^{1}H and 2D HMBC ^{13}C-^{1}H NMR spectra respectively). MS (MALDI-TOF) m/z for $[C_{50}H_{60}BrClN_8O_{15}P]^-$, calcd: 1157.2793; found: 1157.4092.

1. 2. 7. Synthesis of precursor 8: To a solution of compound **II**[9] (0.3 mg, 0.3μmol) in dry DMF (75 μL), DIEA (0.3μL, 1.5 μmol, 5 equiv) and succinimidyl 6-(boc-hydrazine)nicotinate (0.2 mg, 0.6 μmol, 2 equiv) were added. The resulting solution was stirred at room temperature. After 16h, DMF was removed under reduced pressure, the crude mixture was diluted with HClaq (5M, 100 μL) and stirred for an additional 24h at room temperature. The crude pseudo peptide was purified by RP-HPLC in condition 1.

Compound 8 was obtained as white powder (0.16 mg, 47%) after freeze drying. $\varepsilon_{272\ nm}$(MeOH) = 35 185 $cm^{-1}M^{-1}$. Rt = 6.31 min in condition A, Rt = 7.36 min in condition B. The complete ^{1}H and ^{13}C NMR assignments are detailed in Table S7 (see also Figure S11, S12 and S13 for representative ^{1}H, 2D HSQC ^{13}C-^{1}H and 2D HMBC ^{13}C-^{1}H NMR spectra respectively). MS (MALDI-TOF) m/z for $[C_{51}H_{60}BrClN_8O_{14}P]^-$, calcd: 1153.2844; found: 1153.4360.

2. Radiochemistry

The precursors **5**, **6**, **7** and **8** were labeled with [^{99m}Tc]-TcO_4^- following previously described methods, which were empirically optimized. To 10 μg of **5** or **6** in 10 μL of DMSO, the following were added successively: 50 μL of ammonium acetate 0.5 M solution (pH = 8.0), 4 μL of disodium tartrate (5 % solution in 0.5 M ammonium acetate, pH adjusted to 8.5), 10 μL of ammonium acetate 0.25 M, 2 μL of ascorbic acid (0.3 % solution in 10mM HCl) and 2 μL of $SnCl_2$ (0.4 % solution in 10mM HCl, pH=2.5). After removal of air, 100 μL of [^{99m}Tc]-TcO_4^- solution (444–685 MBq) was added and the mixture was heated at 85 °C for 15–30 min.

7 was labeled in a 2-step method using a ^{99m}Tc-carbonyl core intermediate. [^{99m}Tc$(CO)_3(H_2O)_3]^+$ was obtained by mixing the Isolink kit (Paul Scherrer Institute – CRS - Clinical Drug Supply, Switzerland) with ~1200 MBq of [^{99m}Tc]-TcO_4^- and heating the mixture at 95 °C for 20 min. After cooling and neutralization to pH = 7 by adding 1 N HCl, 370 MBq of [^{99m}Tc$(CO)_3(H_2O)_3]^+$ was added to 10 μg of **7** in 10 μL of DMSO and heated at 95 °C for 30 min.

10 μg of **8** in 100 μL of 80 % aqueous ethanol was incubated with 370 MBq of [^{99m}Tc]-TcO_4^- and 100 μL (10 mg) of tricine solution in succinate buffer (25 mM, pH=5.0), in the presence of 20 μL (60) μg of freshly prepared $SnCl_2$ solution in 0.1 N HCl for 10 min at room temperature before adding 120 μL (5.5 mg) of triphenylphosphine-3,3’,3”-trisulfonic acid solution in 25 mM succinate buffer (pH=5.0), and heating the mixture at 100 °C for 30 min.

3. Radiochemical stability assessment

Radiochemical stability of ^{99m}Tc-labeled tracers was evaluated by RP- radio-HPLC analysis following incubation in PBS (for 6 hours at room temperature), or in mouse blood (for 0.5 h, 2 h and 3 h at 37 °C) using plasma after protein precipitation with methanol. The analysis was performed with a dedicated system (HPLC system 2489; Waters) coupled with a radio-detector, using an analytic column (Jupiter, 4 μm Proteo 90 Å; Phenomenex) at a flow rate of 1 mL/min with gradients of solvent A (aqueous solution, 25 mM $HCOONH_4$) and solvent B (90% aqueous acetonitrile, 25 mM $HCOONH_4$). Solvent gradients were: 10 % B for 2–5 min, 10–70 % B in 15 min and 70–90 % B in 5 min or directly 10–90 % B in 18 min and 90 % for 5–10 min (30 min total). Additional analytic methods were tested and failed for [^{99m}Tc]-**4** (not described).

4. Affinity and selectivity evaluation

The inhibition constants of the parent RXP470.1 and the 4 tracers toward a panel of recombinant human metzincins, including human MMP-12, TACE and ADAM-TS4, and murine MMP-12 were determined using a fluorogenic activity assay, as previously described.[9] A typical MMP inhibition assay was performed in 50 mM Tris-HCl buffer, pH = 6.8, 10 mM $CaCl_2$ at 25°C in presence of 0.2–0.5 nM of MMP using a fluorogenic substrate (4.5 μM, Mca-Pro-Leu- Gly-Leu-Dpa-Ala-Arg-NH_2, Enzo Life Sciences). ADAMT-S4 inhibition assays were carried out in 50 mM Tris-HCl buffer, 100 mM NaCl, 10 mM $CaCl_2$, pH 6.8, at 25°C using 5-FAM-Ala-Glu-Lys-Gln-Gly-Arg-Pro-Ile-Ser- Ile-Ala-Lys-TAMRA-

NH_2 substrate (0.9 μM, Enzo Life Sciences) and TACE inhibition assays were carried out in 20 mM Tris-HCl buffer (pH 6.8) at 25°C in presence of MCA-Lys-Pro-Leu-Gly-Leu-Dpa-Ala-Arg-NH2 substrate (4.5 μM, R&D systems). Inhibition assays in the presence of mouse serum albumin (Sigma Aldrich) or human serum albumin (Sigma Aldrich) were performed following the procedure described above. Inhibition assays in diluted mouse plasma were conducted in the presence of a selective MMP-12 substrate developed in our laboratory (Mca-Pro-Leu-Gly-Cys(Mob)-Glu-Glu-Dpa-NH2) at 18 μM. Black, flat-bottomed, 96-well non-binding surface plates (Corning-Costar) were used for these tests. Fluorescence signals were monitored using a Fluoroskan Ascent photon counter spectrophotometer (Thermo-Labsystems) equipped with a temperature control device and a plate shaker. For each compound evaluated, the percentage inhibition was determined at five concentrations in triplicate, within the range between 20–80. Ki values were determined using the method proposed by Horovitz and Leviski.[43]

5. Animal experiments

C57BL/6J-albino mice (originally from the Jackson Laboratory, n = 16) were used to study tracers' biodistribution and blood kinetics. Male $ApoE^{-/-}$ mice (originally from the Jackson Laboratory, n = 23) were infused for 4 weeks with 1000 ng/kg/min of human Ang II (Calbiochem) delivered by a subcutaneous osmotic minipump (Model 2004, Alzet), as described.[35] All experiments were performed in accordance with the regulations of Yale University and VA Connecticut Institutional Animal Care and Use Committees.

5. 1 Biodistribution—Mice were injected intravenously with 22 ± 13 MBq of tracer (n = 4 per tracer) and serial blood samples were collected. Two hours after tracer injection, the animals were euthanized and different tissues were collected and weighted. The tissue and blood radioactivity were recorded (WIZARD2, PerkinElmer), corrected for decay and expressed as %ID/g tissue or %ID/mL blood.

5. 2 Quantitative Autoradiography—$ApoE^{-/-}$ mice surviving 4 weeks of Ang II infusion were injected intravenously with 20.6 ± 5.6 MBq of [^{99m}Tc]-**1** and euthanized under anesthesia after 2 hrs. A subset of animals was injected intravenously with a 1000-fold excess of RYM, a broad-spectrum MMP inhibitor ~2 minutes prior to [^{99m}Tc]-**1** administration.[40] The entire aorta and carotid arteries were dissected under microscope and different tissues were collected to assess biodistribution. The aorta and standards of known activity were placed on a phosphor screen (MultiSensitive Phosphor Screen; PerkinElmer) for autoradiography. The phosphor screen was read using a phosphoimager (Typhoon Trio; GE Healthcare Life Sciences) and the digital images were analyzed using Fiji/ImageJ software (National Institutes of Health).

5. 3 Statistical Analysis—All data are presented as mean ± SD. Datasets from different experimental groups where compared using Student's t-test with or without Welsh's correction depending whether variances were different or equal. The blood activities of different groups of animals were compared using 2-way ANVOA with post hoc Bonferroni adjustment.

Supplementary Material

Refer to Web version on PubMed Central for supplementary material.

ACKNOWLEDGMENTS

This work was supported by National Institutes of Health R01 HL112992, R01 HL138567, and Department of Veterans Affairs Merit Award I01 BX004038.

ABBREVIATIONS USED

AAA	abdominal aortic aneurysm
ADAM-TS4	a disintegrin and metalloproteinase with thrombospondin motifs
BOC	tert-Butyloxycarbonyl
COPD	chronic obstructive pulmonary disease
DCM	dichloromethane
DIEA	N,N-diisopropylethylamine
DMF	dimethylformamide
HCTU	2-(6-Chloro-1-H-benzotriazole-1-yl)-1,1,3,3-tetramethylaminium hexafluorophosphate
HYNIC	6-hydrazinonicotinyl
MAG	mercaptoAcetylGlycyl-glycyl-glycine
MAS	mercaptoAcetylSeryl-seryl-serine
MMPs	matrix metalloproteinases
Mmt	monomethoxy trityl
NMM	N-methylmorpholine
NMP	N-methyl-2-pyrrolidone
PEG	Polyethylene glycol
PSMA	prostate-specific membrane antigen
TACE	tumor necrosis factor-alpha converting enzyme
TFA	trifluoroacetic acid
TFE	trifluoro ethanol

REFERENCES

1. Sternlicht MD; Werb Z How Matrix Metalloproteinases Regulate Cell Behavior. Annu Rev Cell Dev Bi 2001, 17, 463–516.

2. Rodriguez D; Morrison CJ; Overall CM Matrix Metalloproteinases: What Do They Not Do? New Substrates and Biological Roles Identified by Murine Models and Proteomics. Biochim Biophys Acta 2010, 1803, 39–54. [PubMed: 19800373]

3. Nissinen L; Kahari VM Matrix Metalloproteinases in Inflammation. Biochim Biophys Acta 2014, 1840, 2571–2580. [PubMed: 24631662]

4. Page-McCaw A; Ewald AJ; Werb Z Matrix Metalloproteinases and the Regulation of Tissue Remodelling. Nat Rev Mol Cell Bio 2007, 8, 221–233. [PubMed: 17318226]

5. Shapiro SD; Kobayashi DK; Ley TJ Cloning and Characterization of a Unique Elastolytic Metalloproteinase Produced by Human Alveolar Macrophages. J Biol Chem 1993, 268, 23824–23829. [PubMed: 8226919]

6. Shapiro SD; Griffin GL; Gilbert DJ; Jenkins NA; Copeland NG; Welgus HG; Senior RM; Ley TJ Molecular Cloning, Chromosomal Localization, and Bacterial Expression of a Murine Macrophage Metalloelastase. J Biol Chem 1992, 267, 4664–4671. [PubMed: 1537850]

7. Lagente V; Le Quement C; Boichot E Macrophage Metalloelastase (MMP-12) as a Target for Inflammatory Respiratory Diseases. Expert Opin Ther Tar 2009, 13, 287–295.

8. Curci JA; Liao S; Huffman MD; Shapiro SD; Thompson RW Expression and Localization of Macrophage Elastase (Matrix Metalloproteinase-12) in Abdominal Aortic Aneurysms. J Clin Invest 1998, 102, 1900–1910. [PubMed: 9835614]

9. Bordenave T; Helle M; Beau F; Georgiadis D; Tepshi L; Bernes M; Ye Y; Levenez L; Poquet E; Nozach H; Razavian M; Toczek J; Stura EA; Dive V; Sadeghi MM; Devel L Synthesis and in Vitro and in Vivo Evaluation of MMP-12 Selective Optical Probes. Bioconjug Chem 2016, 27, 2407–2417. [PubMed: 27564088]

10. Razavian M; Bordenave T; Georgiadis D; Beau F; Zhang J; Golestani R; Toczek J; Jung JJ; Ye Y; Kim HY; Han J; Dive V; Devel L; Sadeghi MM Optical Imaging of MMP-12 Active Form in Inflammation and Aneurysm. Sci Rep 2016, 6, 38345. [PubMed: 27917892]

11. Longo GM; Buda SJ; Fiotta N; Xiong WF; Griener T; Shapiro S; Baxter BT MMP-12 Has a Role in Abdominal Aortic Aneurysms in Mice. Surgery 2005, 137, 457–462. [PubMed: 15800495]

12. Wang Y; Ait-Oufella H; Herbin O; Bonnin P; Ramkhelawon B; Taleb S; Huang J; Offenstadt G; Combadiere C; Renia L; Johnson JL; Tharaux PL; Tedgui A; Mallat Z TGF-Beta Activity Protects Against Inflammatory Aortic Aneurysm Progression and Complications in Angiotensin II-Infused Mice. J Clin Invest 2010, 120, 422–432. [PubMed: 20101093]

13. Toczek J; Ye Y; Gona K; Kim HY; Han J; Razavian M; Golestani R; Zhang J; Wu TL; Jung JJ; Sadeghi MM Preclinical Evaluation of RYM1, a Matrix Metalloproteinase-Targeted Tracer for Imaging Aneurysm. J Nucl Med 2017, 58, 1318–1323. [PubMed: 28360209]

14. Scholtes VP; Johnson JL; Jenkins N; Sala-Newby GB; de Vries JP; de Borst GJ; de Kleijn DP; Moll FL; Pasterkamp G; Newby AC Carotid Atherosclerotic Plaque Matrix Metalloproteinase-12-Positive Macrophage Subpopulation Predicts Adverse Outcome After Endarterectomy. J Am Heart Assoc 2012, 1, e001040. [PubMed: 23316311]

15. Morita H; Nagai R MMP12, lung function, and COPD in high-risk populations. N Engl J Med 2010, 362, 1241; author reply 1242.

16. Hunninghake GM; Cho MH; Tesfaigzi Y; Soto-Quiros ME; Avila L; Lasky-Su J; Stidley C; Melen E; Soderhall C; Hallberg J; Kull I; Kere J; Svartengren M; Pershagen G; Wickman M; Lange C; Demeo DL; Hersh CP; Klanderman BJ; Raby BA; Sparrow D; Shapiro SD; Silverman EK; Litonjua AA; Weiss ST; Celedon JC MMP12, Lung Function, and COPD in High-Risk Populations. N Engl J Med 2009, 361, 2599–2608. [PubMed: 20018959]

17. Chaudhuri R; McSharry C; Brady J; Donnelly I; Grierson C; McGuinness S; Jolly L; Weir CJ; Messow CM; Spears M; Miele G; Nocka K; Crowther D; Thompson J; Brannigan M; Lafferty J; Sproule M; Macnee W; Connell M; Murchison JT; Shepherd MC; Feuerstein G; Miller DK; Thomson NC Sputum Matrix Metalloproteinase-12 in Patients with Chronic Obstructive Pulmonary Disease and Asthma: Relationship to Disease Severity. J Allergy Clin Immunol 2012, 129, 655–663 e8. [PubMed: 22305682]

18. Vandenbroucke RE; Libert C Is There New Hope for Therapeutic Matrix Metalloproteinase Inhibition? Nat Rev Drug Discov 2014, 13, 904–927. [PubMed: 25376097]

19. Zhong Y; Lu YT; Sun Y; Shi ZH; Li NG; Tang YP; Duan JA Recent Opportunities in Matrix Metalloproteinase Inhibitor Drug Design for Cancer. Expert Opin Drug Discov 2018, 13, 75–87. [PubMed: 29088927]

20. Liu J; Khalil RA Matrix Metalloproteinase Inhibitors as Investigational and Therapeutic Tools in Unrestrained Tissue Remodeling and Pathological Disorders. Prog Mol Biol Transl 2017, 148, 355–420.

21. Levin M; Udi Y; Solomonov I; Sagi I Next Generation Matrix Metalloproteinase Inhibitors - Novel Strategies Bring New Prospects. Bba-Mol Cell Res 2017, 1864, 1927–1939.

22. Iyer RP; Patterson NL; Fields GB; Lindsey ML The History of Matrix Metalloproteinases: Milestones, Myths, and Misperceptions. Am J Physiol Heart Circ Physiol 2012, 303, H919–930. [PubMed: 22904159]

23. Radisky ES; Raeeszadeh-Sarmazdeh M; Radisky DC Therapeutic Potential of Matrix Metalloproteinase Inhibition in Breast Cancer. J Cell Biochem 2017, 118, 3531–3548. [PubMed: 28585723]

24. Devel L; Czarny B; Beau F; Georgiadis D; Stura E; Dive V Third Generation of Matrix Metalloprotease Inhibitors: Gain in Selectivity by Targeting the Depth of the S1' Cavity. Biochimie 2010, 92, 1501–1508. [PubMed: 20696203]

25. Devel L; Rogakos V; David A; Makaritis A; Beau F; Cuniasse P; Yiotakis A; Dive V Development of Selective Inhibitors and Substrate of Matrix Metalloproteinase-12. J Biol Chem 2006, 281, 11152–11160. [PubMed: 16481329]

26. Johnson JL; Devel L; Czarny B; George SJ; Jackson CL; Rogakos V; Beau F; Yiotakis A; Newby AC; Dive V A Selective Matrix Metalloproteinase-12 Inhibitor Retards Atherosclerotic Plaque Development in Apolipoprotein E-Knockout Mice. Arterioscler Thromb Vasc Biol 2011, 31, 528–535. [PubMed: 21212406]

27. Lim NH; Meinjohanns E; Bou-Gharios G; Gompels LL; Nuti E; Rossello A; Devel L; Dive V; Meldal M; Nagase H In Vivo Imaging of Matrix Metalloproteinase 12 and Matrix Metalloproteinase 13 Activities in the Mouse Model of Collagen-Induced Arthritis. Arthritis Rheumatol 2014, 66, 589–598. [PubMed: 24574219]

28. Marchant DJ; Bellac CL; Moraes TJ; Wadsworth SJ; Dufour A; Butler GS; Bilawchuk LM; Hendry RG; Robertson AG; Cheung CT; Ng J; Ang L; Luo Z; Heilbron K; Norris MJ; Duan W; Bucyk T; Karpov A; Devel L; Georgiadis D; Hegele RG; Luo H; Granville DJ; Dive V; McManus BM; Overall CM A New Transcriptional Role for Matrix Metalloproteinase-12 in Antiviral Immunity. Nat Med 2014, 20, 493–502. [PubMed: 24784232]

29. Iyer RP; Patterson NL; Zouein FA; Ma Y; Dive V; de Castro Bras LE; Lindsey ML Early Matrix Metalloproteinase-12 Inhibition Worsens Post-Myocardial Infarction Cardiac Dysfunction by Delaying Inflammation Resolution. Int J Cardiol 2015, 185, 198–208. [PubMed: 25797678]

30. Ella E; Harel Y; Abraham M; Wald H; Benny O; Karsch-Bluman A; Vincent D; Laurent D; Amir G; Izhar U; Shapira OM; Yoon D; Lee HS; Sugarbaker DJ; Burt B; Peled A; Wald O Matrix Metalloproteinase 12 Promotes Tumor Propagation in the Lung. J Thorac Cardiov Sur 2018, 155, 2164–2175.

31. Dufour A; Bellac CL; Eckhard U; Solis N; Klein T; Kappelhoff R; Fortelny N; Jobin P; Rozmus J; Mark J; Pavlidis P; Dive V; Barbour SJ; Overall CM C-Terminal Truncation of IFN-Gamma Inhibits Proinflammatory Macrophage Responses and Is Deficient in Autoimmune Disease. Nat Commun 2018, 9, 2416. [PubMed: 29925830]

32. Butsch V; Borgel F; Galla F; Schwegmann K; Hermann S; Schafers M; Riemann B; Wunsch B; Wagner S Design, (Radio)Synthesis, and in Vitro and in Vivo Evaluation of Highly Selective and Potent Matrix Metalloproteinase 12 (MMP-12) Inhibitors as Radiotracers for Positron Emission Tomography. J Med Chem 2018, 61, 4115–4134. [PubMed: 29660282]

33. Kondo N; Temma T; Aita K; Shimochi S; Koshino K; Senda M; Iida H Development of Matrix Metalloproteinase-Targeted Probes for Lung Inflammation Detection with Positron Emission Tomography. Sci Rep-Uk 2018, 8, 1347.

34. Hagimori M; Temma T; Kudo S; Sano K; Kondo N; Mukai T Synthesis of Radioiodinated Probes Targeted Toward Matrix Metalloproteinase-12. Bioorg Med Chem Lett 2018, 28, 193–195. [PubMed: 29191557]

35. Golestani R; Razavian M; Nie L; Zhang J; Jung JJ; Ye Y; de Roo M; Hilgerink K; Liu C; Robinson SP; Sadeghi MM Imaging Vessel Wall Biology to Predict Outcome in Abdominal Aortic Aneurysm. Circ Cardiovasc Imaging 2015, 8, e002471 [PubMed: 25550400]

36. Lagisetty P; Vilekar P; Awasthi V Synthesis of Radiolabeled Cytarabine Conjugates. Bioorg Med Chem Lett 2009, 19, 4764–4767. [PubMed: 19574048]

37. Wang Y; Liu G; Hnatowich DJ Methods for MAG3 Conjugation and 99mTc Radiolabeling of Biomolecules. Nat Protoc 2006, 1, 1477–1480. [PubMed: 17406438]

38. Liu S; Edwards DS; Harris AR; Ziegler MC; Poirier MJ; Ewels BA; Diluzio WR; Hui P Towards Developing a Non-SnCl2 Formulation for RP444, a New Radiopharmaceutical for Thrombus Imaging. J Pharm Sci 2001, 90, 114–123. [PubMed: 11169528]

39. Badar A; Williams J; de Rosales RT; Tavare R; Kampmeier F; Blower PJ; Mullen GE Optimising the Radiolabelling Properties of Technetium Tricarbonyl and His-Tagged Proteins. EJNMMI Res 2014, 4, 14. [PubMed: 24606843]

40. Ye YP; Toczek J; Gona K; Kim HY; Han J; Razavian M; Golestani R; Zhang JS; Wu TL; Ghosh M; Jung JJ; Sadeghi MM Novel Arginine-containing Macrocyclic MMP Inhibitors: Synthesis, Tc-99m-labeling, and Evaluation. Sci Rep-Uk 2018, 8, 11647.

41. Ray Banerjee S; Pullambhatla M; Foss CA; Falk A; Byun Y; Nimmagadda S; Mease RC; Pomper MG Effect of Chelators on the Pharmacokinetics of (99m)Tc-Labeled Imaging Agents for the Prostate-Specific Membrane Antigen (PSMA). J Med Chem 2013, 56, 6108–6121. [PubMed: 23799782]

42. Boyd G Technetium and Promethium. J Chem Educ 1959, 36, 3–14.

43. Horovitz A; Levitzki A An Accurate Method for Determination of Receptor-Ligand and Enzyme-Inhibitor Dissociation Constants from Displacement Curves. Proc Natl Acad Sci U S A 1987, 84, 6654–6658. [PubMed: 3477796]

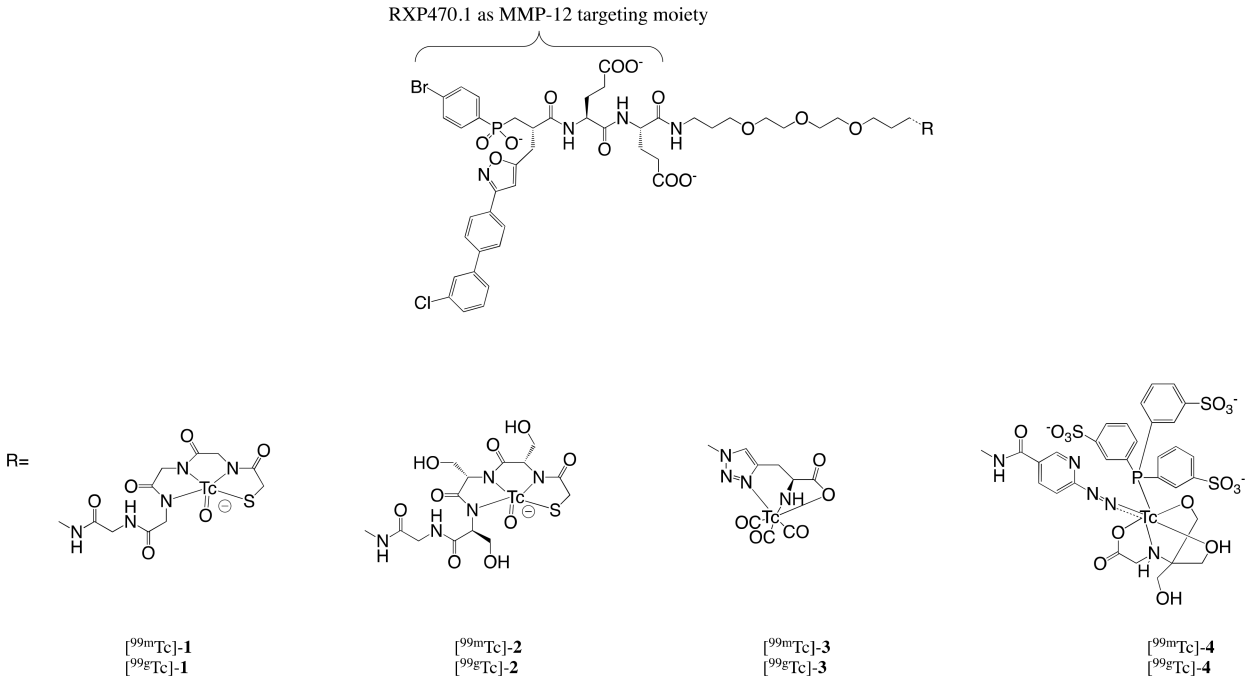

Figure 1.
Chemical structures of Tc-labeled MMP-12 targeting tracers with a RXP470.1 scaffold.

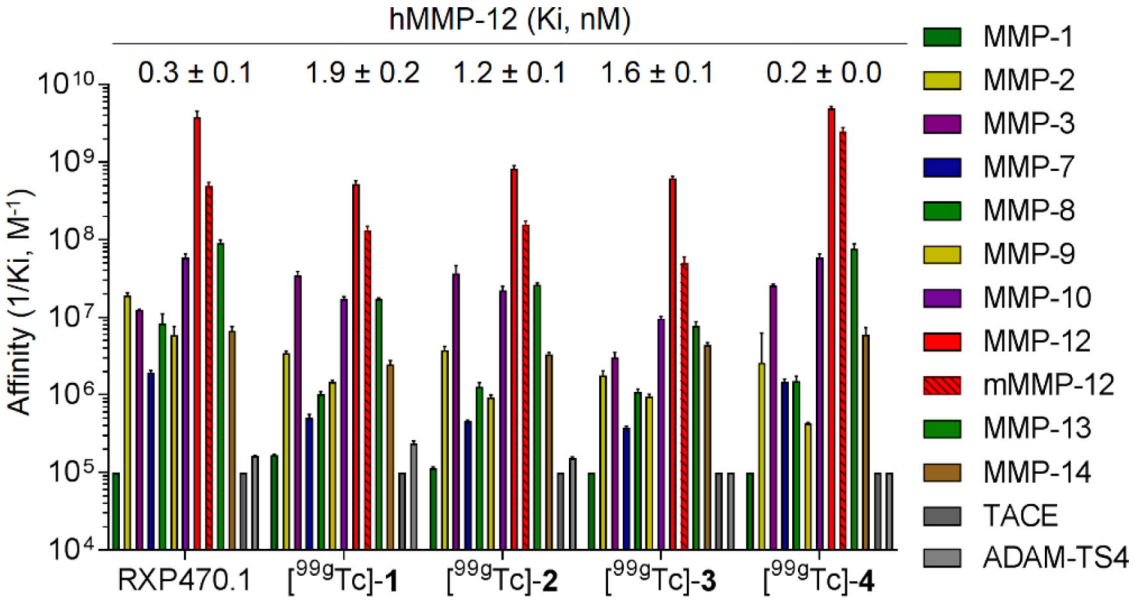

Figure 2:

Comparison of affinity selectivity profiles between RXP470.1 and [^{99g}Tc]-**1** to **4** towards a panel of ten human MMPs (hMMP-1, 2, 3, 7, 8, 9, 10, 12, 13 and 14), two human metzincins (hTACE and hADAM-TS4) and murine MMP12 (mMMP-12). Each metalloprotease is associated to a color code (right panel). Ki (M) values were determined in 50 mM Tris-HCl buffer, pH 6.8 with 10 mM $CaCl_2$ at 25°C. Ki values are the mean ± SD for three independent experiments. The 1/Ki values are reported in logarithmic scale.

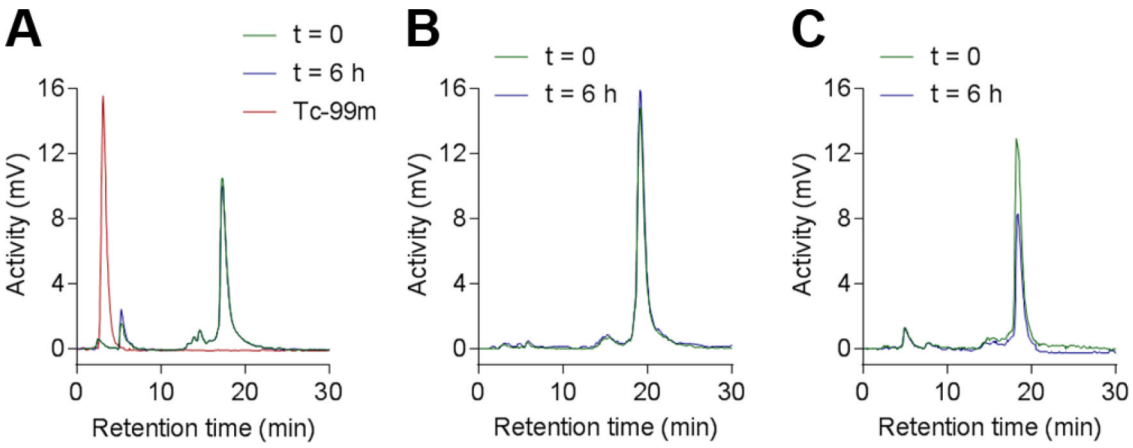

Figure 3.

Radio-HPLC profiles of [^{99m}Tc]-**1** (A), [^{99m}Tc]-**2** (B) and [^{99m}Tc]-**3** (C) right after the radiolabeling (green plot) and after 6 h (blue plot) of incubation at room temperature in PBS.

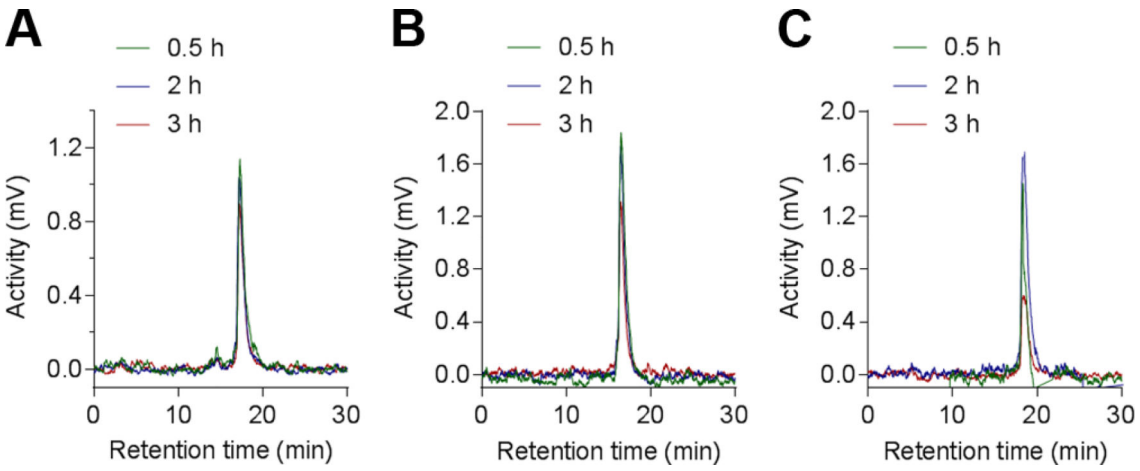

Figure 4.

Radio-HPLC profiles of [^{99m}Tc]-**1** (A), [^{99m}Tc]-**2** (B) and [^{99m}Tc]-**3** (C) incubated in mouse blood at 37°C and collected at different time points (0.5 h-green plot, 2 h-blue plot and 3 h-red plot).

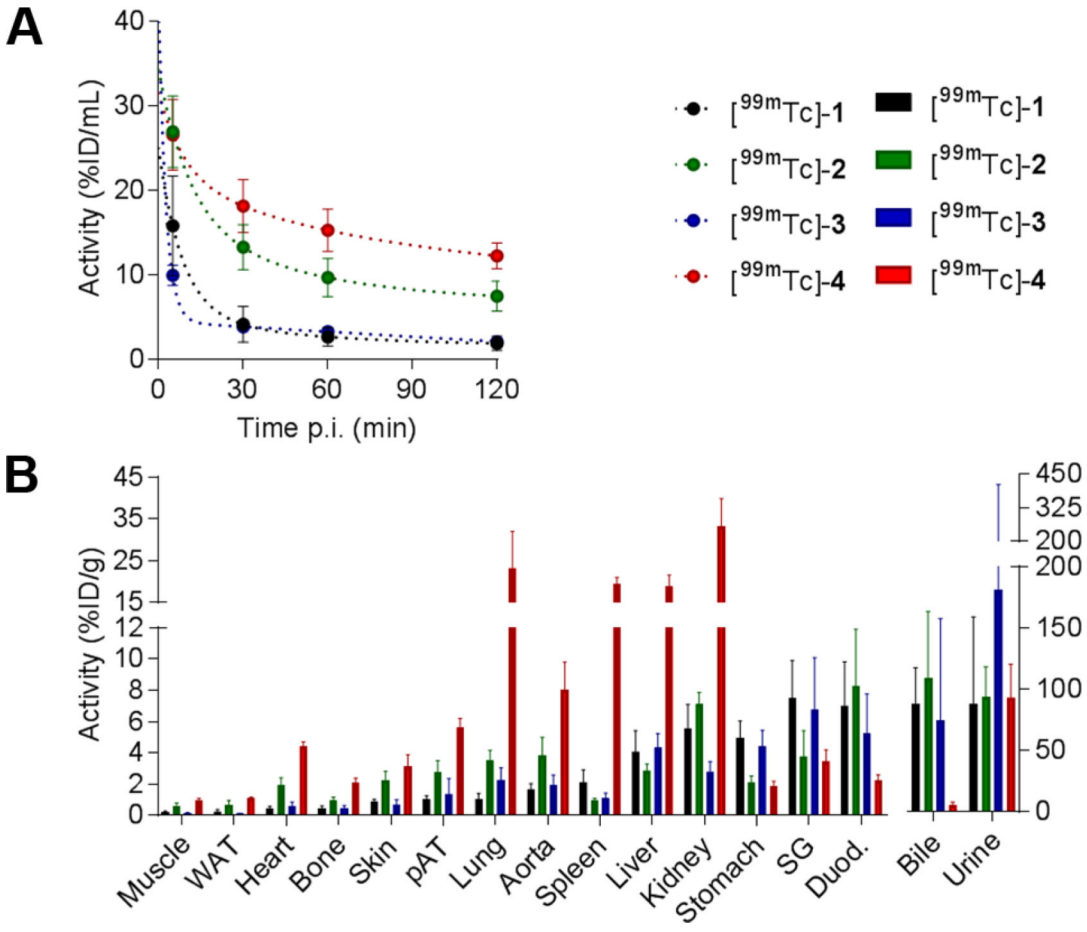

Figure 5.

Tracer biodistribution and clearance. Blood kinetics (A) and biodistribution at 2 hours (B) of [^{99m}Tc]-**1** (black), [^{99m}Tc]-**2** (green), [^{99m}Tc]-**3** (blue), and [^{99m}Tc]-**4** (red) in mice. n = 4 in each group. ID: injected dose, WAT: white adipose tissue, pAT: periaortic adipose tissue, SG: salivary glands, Duod.: duodenum.

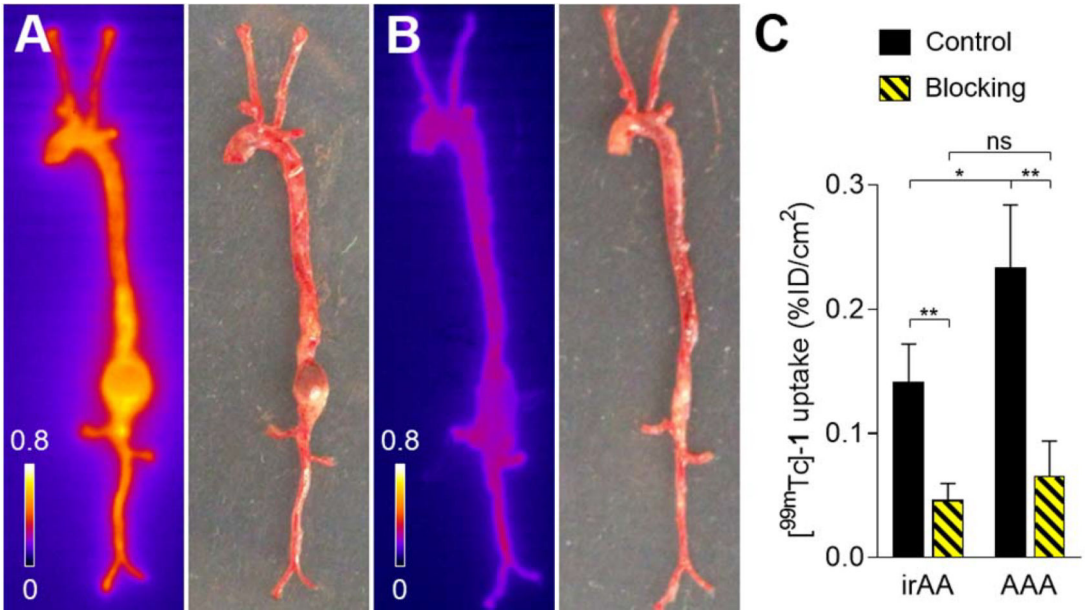

Figure 6.

Autoradiography and macroscopic picture of aortae from apoE$^{-/-}$ mice with AAA at 4 weeks of Ang II infusion harvested 2 h after the injection of [^{99m}Tc]-**1** (A, Control, n = 4) or [^{99m}Tc]-**1** and 1000-fold excess of a broad-spectrum MMP inhibitor (B, Blocking, n = 3). Quantification of [^{99m}Tc]-**1** uptake in non-remodeled infra-renal abdominal aorta (irAA) and AAA (C). * $P < 0.05$, ** $P < 0.01$.

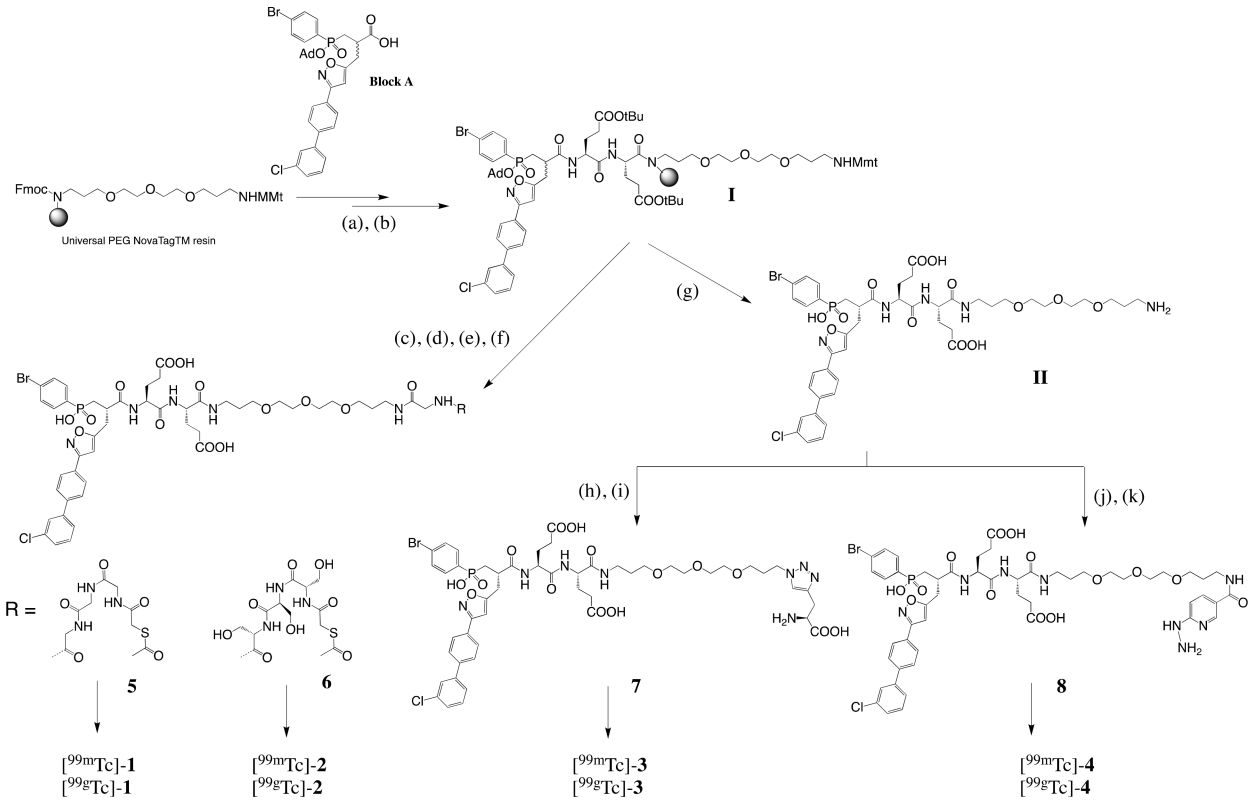

Scheme 1.

Synthesis of precursors **5**, **6**, **7** and **8** to access ^{99g}Tc and ^{99m}Tc derivatives.